MACHINE-LEARN-DRIVEN PREDICTION OF STREAMWISE VORTICITY INDUCED BY A RANDOM DISTRIBUTED ROUGHNESS PATCH IN HYPERSONIC FLOW

Friedrich Ulrich and Christian Stemmer

Technical University of Munich
Chair of Aerodynamics and Fluid Mechanics
Boltzmannstr. 15, 85748 Garching b. München, Germany.

ABSTRACT

Boundary-layer transition on the surface of a space transportation vehicle highly influences the heat-flux the thermal protection system has to withstand in a re-entry scenario. Distributed surface roughness can cause cross-flow like vortices in the wake of the roughness patch that highly destabilize the flow regime. The variety of roughness parameters which influence the generation of a cross-flow vortex is addressed with the training of a Deep Neural Network. This paper presents a database of Direct Numerical Simulations (DNS) of a restricted domain of an Apollo-like space capsule with different distributed roughness patches. This study is using machine learning to predict the streamwise vorticity of a cross-flow-like vortex generated by a distributed random roughness patch. A sensitivity analysis identifies the importance of surface derivatives and the location of the maximum and minimum peak in the roughness patch.

***Index Terms*—** Hypersonic Flow, Machine Learning, Distributed Roughness, Re-entry Capsule

1. INTRODUCTION

A space transportation vehicle requires a thermal protection system (TPS) in order to withstand the heat load in a re-entry scenario. The heat flux depends on the flow regime on the surface of the space capsule. In case of a laminar to turbulent transition, the heat flux can be increased by a factor of ten [1]. It is therefore a mission-critical aspect to properly model the laminar-turbulent transition in the hypersonic flow regime. During the re-entry of a space capsule, a surface roughness on the heat shield is the most-likely cause for laminar-turbulent transition as the accelerated flow is modally stable and transient growth is unlikely [2].

Schneider [3] presents in an overview on the experimental investigation of surface roughness in hypersonic flow. On the numerical side, several studies investigated the effect of isolated roughness elements in hypersonic transition. Among others, Padilla Montero and Pinna [4] investigated the role of isolated roughness elements in a laminar boundary layer at Mach 6. Two different roughness geometries, a sharp-edged cubical element and a three-dimensional sharp-edged ramp, were investigated. The isolated element produced a pair of counter-rotating vortices in the wake which generates strong velocity gradients leading to a three-dimensional shear-layer. The streamwise evolution of the wake instabilities are investigated through a temporal growth-rate decomposition. The majority of potential energy within the roughness-induced instabilities in the wake is gained by the transport of disturbance entropy across temperature gradients in the base flow.

A new cross-flow like vortex induced by a distributed roughness patch was observed by Di Giovanni and Stemmer [5] at M = 5.9 flow of a blunt capsule configuration. The roughness induced cross-flow showed higher amplification rates in comparison with counter-rotation vortices in the wake of a spanwise periodic roughness element with the same maximum height. The authors emphasize the necessity to include the roughness shape into a future transition criteria.

In order to better understand the role of the roughness topology of distributed patches, Ulrich and Stemmer [6] investigate two different types of random roughnesses with a sinusoidal and triangular base function. Stronger streamwise vorticity is computed for the triangular base-function patches. In a 2D Fourier transformation, the growth of acoustic disturbances is investigated in the wake of both roughness types. The stronger vortex in the triangular case generates stronger wall-normal and spanwise gradients leading to transition further upstream.

Brunton *et al.* [7] provide an overview of the usage of machine learning (ML) in the field of fluid mechanics and point out the potential this method provides. The prediction of Nikuradse equivalent sand-grain height k_s with a Deep Neural Network (DNN) and Gaussian Process Regression (GPR) is proposed by Jouybari *et al.* [8] in order to understand influence of a rough surface topology on turbulent flow. The machine learning models were able to predict the equivalent sand-grain height with an average error of less then 10%. The ML approach was significantly better than polynomial models. Further, the author see the potential to compute physics-related flow quantities, e.g. flow separation locations, with their database in the future.

Lee *et al.* [9] improve the estimation of the drag on irregular rough surfaces with a transfer learning-step. In a pre-training step, the neural network is learning known surface statistics which have an influence on the drag. The 'approximated knowledge' is then fine-tuned in a second step. The proposed transfer framework is adapting the drag model on empirical data and therefore requires only a limited number of computationally demanding Direct Numerical Simulations. Despite the improvement of the prediction error by the pre-step, the database should be increased for the generalization ability of the framework.

The influence of a distributed roughness element on the wake flow presents a parameter-rich problem which requires a large database of computationally expensive Direct Numerical Simulations. We present a database of such simulations with over 4830 simulations which makes it one of the largest databases for distributed roughness patches in the hypersonic flow regime. Further, we describe the possibilities and challenges to predict the maximum vorticity in the roughness wake.

2. GOVERNING EQUATIONS

This study used a database of DNS which are computed using the compressible Navier-Stokes equations in three dimensions. This includes the continuity equation,

$$\frac{\partial \rho}{\partial t} + \frac{\partial}{\partial x_i}\left(\rho u_i\right) = 0, \tag{1}$$

with the density ρ and the velocity component u in the Einstein notation. Further, we use the following momentum equations:

$$\frac{\partial}{\partial t}\left(\rho u_i\right) + \frac{\partial}{\partial x_j}\left(\rho u_i u_j\right) = -\frac{\partial p}{\partial x_i} + \frac{\partial \sigma_{ij}}{\partial x_j}, \tag{2}$$

with the spatial coordinates x_i and the time t. The stress tensor σ_{ij} is computed with the viscosity μ and

$$\sigma_{ij} = \mu\left[\left(\frac{\partial u_i}{\partial x_j} - \frac{\partial u_j}{\partial x_i}\right) - \frac{2}{3}\frac{\partial u_k}{\partial x_k}\right]. \tag{3}$$

The energy equation,

$$\frac{\partial \rho E}{\partial t} + \frac{\partial}{\partial x_j}\left[\left(\rho E + p\right) u_j\right] = \frac{\partial}{\partial x_j}\left(\sigma_{ij} u_j\right) + \frac{\partial}{\partial x_j}\left(\lambda \frac{\partial T}{\partial x_j}\right), \tag{4}$$

this system is closed with a chemical gas model which takes high temperature effects into account and provides the equilibrium temperature and composition for the ideal gas equation of state for the individual species.

This study uses a five species gas model (N_2, O_2, NO, N, O) proposed by Park [10] to compute the transport and thermodynamic properties of the fluid in chemical equilibrium. Since this investigation is focusing on the prediction of streamwise vorticity computational more demanding chemical models, such as chemical (and thermal) non-equilibrium, are not used. This simplification can be justified, because the influence of the gas model on the velocity field is much smaller compared to its influence on the thermal boundary layer. A detailed comparison between the different gas models can be found in [11, 12].

3. DATABASE SETUP

The training dataset is generated with a large number of DNS calculations. These simulations investigate a restricted domain (see Section 3.1) on the surface of an Apollo-like capsule. Each domain is equipped with a random roughness patch which is described in Section 3.3. The distributed roughness patch generates a cross-flow like vortex in the wake of the roughness. The maximum streamwise vorticity is measured in a y-z-slice at the outflow of the domain. The maximum vorticity values along with geometrical roughness parameters (see Section 3.4) are stored in the database are used to train, test and validate the DNN.

3.1. Computational Domain

This study investigates the influence of random roughness patches in a restricted domain on the heat shield of an Apollo-like capsule. The inflow conditions of this domain were derived from a 2D DNS of a Mach 20 flow with a zero angle of attack at an altitude of 60 km. The domain is refined in the bow-shock region and has a symmetry line through the stagnation point. A schematic drawing of the 2D domain can be found in Fig. 1 a. The initial conditions for this 2D simulation can be found in Tab. 1. From the results of the 2D simulation,

Table 1. Freestream-conditions for the re-entry Simulation

Parameter	Value	Comment
Mach	20	-
p_∞	29.9	Pa
T_∞	253.3	K
T_{Wall}	1800	K
Re_∞	$1.97 \cdot 10^6$	m^{-1}

the inflow conditions of the restricted domain are derived.

The restricted domain is located in the shoulder region of the space capsule at an angular extension from $\theta_1 = 35.3° - 38.0°$. A detailed description of the two domains can be found in [6].

The reduced domain has a streamwise extension of 28 cm and is 17 cm wide in the spanwise direction. The maximum domain height is 6.6 cm. The grid resolution was set to $i = 85$ (streamwise direction), $j = 69$ (wall-normal direction) $k = 200$ (spanwise direction) with a total number of grid points of 1,173,000. The resolution of the domain was tested by a

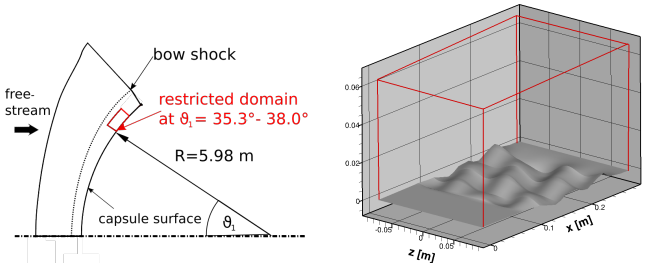

(a) full 2D domain (b) restricted domain

Fig. 1. Sketch of the restricted and reduced restricted domain.

grid convergence study. This study ensured that the value of maximum of streamwise vorticity downstream of the roughness patch was not effected by the chosen grid resolution. The grid points in the wall-normal direction were distributed in a finer fashion to fully resolve the boundary-layer and the cross-flow-like vortex.

3.2. Numerical Solver

All DNS are performed with the semi-commercial code *Navier-Stokes-Mutli-Block Solver* (NSMB). Di Giovanni and Stemmer successfully used this finite volume solver [5] and validated its usage in the current configuration. A documentation of the code can be found in [13]. The program is using the *Message Passing Interface* (MPI) to parallelize the simulation.

The current domain is divided into 560 blocks which are handled on 20 nodes with 28 CPUs. A fourth-order accuracy central scheme is used for the spatial discretization. We computed steady simulations with an implicit Eulerian method based on a Lower-Upper (LU) symmetric Gauss-Seidel method for the time-integration.

Further, we analyzed how the maximum streamwise vorticity is deviating from the converged value, where the L_2 criteria of the density is below 10^{-12}. As the L_2 criterion continues to converge, the maximum of the streamwise vorticity gets closer to the final converged value. We chose to stop the convergence of the DNS within the database at a value of $L_2 < 10^{-7}$. The achieved precision of the streamwise vorticity (10^{-5}) is high enough, especially since the prediction capabilities of a neural network are several orders of magnitude less.

3.3. Random Roughness Patches

Besides the grid resolution and the convergence criteria, the domain size was carefully chosen to only incorporate an area of interest to reduce computational time. Hence, the domain ends shortly (0.02 m) downstream of the roughness patch and does not simulate the downstream development of the cross-flow vortex in the wake.

The database consists of a set of 4830 DNS of the same restricted domain with different random roughness patches. All distributed roughnesses are composed of three sinusoidal waves in spanwise and streamwise direction with a random amplitude and phase. A normalization process ensures that all patches have the same maximum peak height of 18% of the boundary layer height δ in the smooth case.

The distributed roughness h is defined in the following way:

$$h(x,z) = h_{max} \cdot g(x) \sum_{q=1}^{3} \sum_{r=1}^{3} A_{q,r} sin\left(\frac{2\pi q}{\lambda_0} x + \frac{2\pi r}{\lambda_0} z + \phi_{q,r}\right), \tag{5}$$

with a maximum roughness height of $h_{max} = 4.3$ mm and the polynomial smoothing function $g(x)$ which ensures a continuous transition from the smooth capsule surface to the roughness patch. The patch is composed by random sinusoidal waves with an amplitude $A_{q,r} \in [0,1]$ and the phase $\phi_{q,r} \in [0,2\pi]$. However, certain amplitudes are assigned with the value zero to ensure the presence of a minimal wavelength, if $n^2 + m^2 \geq N^2 + 1$. The fundamental roughness-wavelength $\lambda_0 = 170$ mm is referring to the spanwise extension of the domain. Further, the smooth capsule surface is at a height of zero.

3.4. Geometrical Input Parameter

We chose several statistical values as input parameters derived from geometrical parameter of the roughness surface. We computed the average roughness heights h_{avg},

$$h_{avg} = \frac{1}{N_i \cdot N_k} \sum_{i,k} h(i,k), \tag{6}$$

with the number of points N_i,N_k in the streamwise and spanwise directions, respectively. The average value was also computed for the derivative in the streamwise direction

$$\frac{\partial h(i,k)}{\partial i} \tag{7}$$

the derivative in the spanwise direction,

$$\frac{\partial h(i,k)}{\partial k}, \tag{8}$$

the mean curvature,

$$curv(h(i,k))_{mean} = 0.5 \left(\frac{\partial h(i,k)}{\partial i} + \frac{\partial h(i,k)}{\partial k}\right), \tag{9}$$

and the Gaussian curvature,

$$curv(h(i,k))_{gauss} = \left(\frac{\partial h(i,k)}{\partial i} \cdot \frac{\partial h(i,k)}{\partial k}\right). \tag{10}$$

Further, we computed the root-mean square (RMS) of the height

$$h_{rms} = \sqrt{\frac{1}{N_i \cdot N_k} \sum_{i,k} \left(h(i,k) - h_{avg}\right)^2}, \tag{11}$$

as well as the rms-values accordingly with the stream- and spanwise derivative and the mean and Gaussian curvature. Also the skewness was computed from the height and the other geometrical factors,

$$Sk(h) = \frac{1}{h_{rms}^3} \left(\frac{1}{N_i \cdot N_k} \sum_{i,k} \left(h(i,k) - h_{avg}\right)^3 \right). \quad (12)$$

With the skewness value of the streamwise derivative, we compute the streamwise inclination angle

$$I_i = tan^{-1} \left(0.5 \cdot Sk \left(\frac{\partial h(i,k)}{\partial i} \right) \right) \quad (13)$$

and accordingly in the spanwise direction,

$$I_k = tan^{-1} \left(0.5 \cdot Sk \left(\frac{\partial h(i,k)}{\partial k} \right) \right). \quad (14)$$

We also included the position of the roughness maximum height $Pos_{max,i}$ and minimum $Pos_{min,i}$ in streamwise and spanwise coordinates ($Pos_{max,j}$,$Pos_{min,k}$).
Hence, we feed the neural network with a total of 26 different parameters derived from the surface function (Eq. 5) of an individual roughness surface. No additional simulations are performed to compute these parameters.

4. NEURAL NETWORK STRUCTURE

This investigation uses a Deep Neural Network with an input-layers, several hidden layer and an output layer. The aim of the DNN is to solve a regression problem by predicting the continuous value of the maximum streamwise vorticity in the wake.
The network is trained with a random selection (80%) of the simulations. The input parameters are normalized in the first layer. Then the data is processed in three hidden layers with 512 neurons each. After each neuron, the information is passed though an *Exponential Linear Unit* (elu) activation function. Finally, a single value as a result will be computed in the output layer. An overview of the network structure is given in Fig. 2.

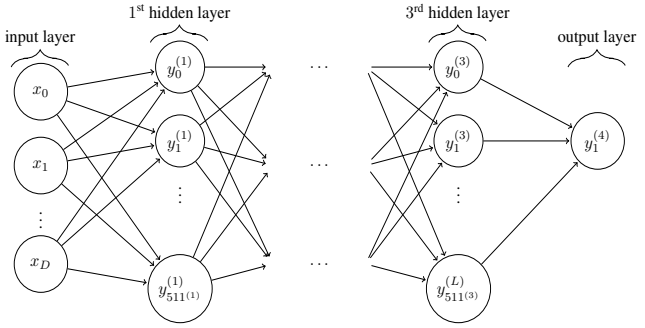

Fig. 2. Network graph of the used DNN

5. RESULTS

5.1. Steady Baseflow

First, we want to discuss some of the DNS results of the DNS database. This supports the understanding of the physical process behind the cross-flow formation.
Two random samples are chosen from the database. In Fig. 3, the roughness surface of the two patches is displayed. The roughness height is colored to highlight peaks and valleys of the patch. The interaction with the random distributed roughness patch leads to the formation of a cross-flow vortex in the wake. The streamwise vorticity ω_x is displayed as a contour plot in a y-z-slice at the end of the domain. Further, a streamline through the vortex core of the strongest cross-flow vortex is drawn at $x = 0.28$ m.
For both patches, the strongest vortex is observed downstream the highest peak in the patch. The peak is forcing fluid in a upward motion and the adjacent valley downstream the highest peak is inducing a spanwise velocity which forms the vortex. Also the streamline of the vortex core passes through this valley. The streamline in Fig. 3a is displaced about 30% further in the (negative) spanwise direction than in the patch in Fig. 3b. The maximum streamwise vorticity is 30% higher compared to patch sample a, but the vortex is 8% closer to the wall. An overview of the position and the magnitude of the strongest cross-flow vortex in the wake for both patches can be found in Tab. 2.
Two vortices are formed for both patches in the wake. The small vortex is located in close proximity to the wall, while the strongest cross-flow like vortex is detached from the surface. Di Giovanni and Stemmer [5] identified this vortex as the dominating source of instability in the wake.

Table 2. Vortices of two random samples

Grid	ω_x [1/s]	y-Position of the vortex core [mm]	z-Position of the vortex core [mm]
a	135,062.7	9.18	-53.83
b	174,474.1	8.49	28.03

5.2. Neural Network Performance

Identifying a relation between the vorticity magnitude and geometrical roughness parameters remains a challenge. In a previous study [6], we have identified the importance of stream- and spanwise derivatives, but on a smaller set of simulations. A precise physical relation between the geometrical parameters and the streamwise vorticity with a single or a few parameters was not possible for this database. The problem is highly nonlinear and parameter rich, hence the prediction ca-

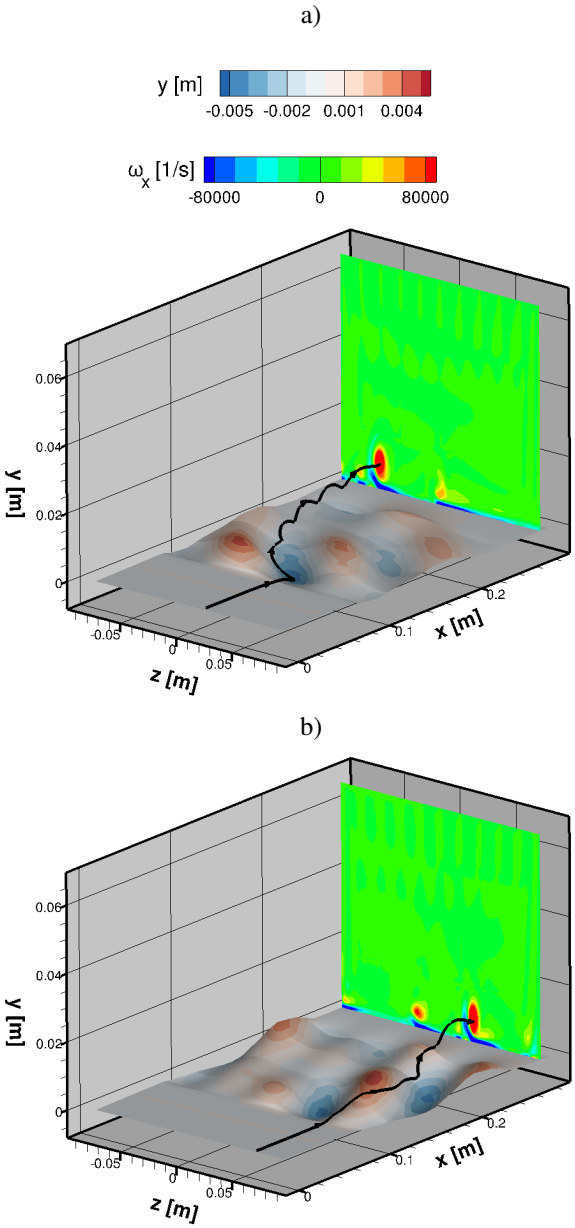

Fig. 3. Streamline of the cross-flow vortex and y-z-slice of streamwise vorticity for two random roughness patches

pability of a DNN was tested.
From the original database, 20% of the simulations were used to test the prediction performance of the network. This randomly selected data was not processed by the DNN before. With the proposed input parameter, the DNN predicted the streamwise vorticity with an average error of 20.7% with only 30 percent exceeding the average error. About one third of the test data is predicted with a relative error under 10%. However, around 10 grids were predicted very poorly with a maximum error of 187%. An overview of the relative error distribution is given in Fig. 5.2b.

The simulated or *true* vorticity values are plotted against the predicted values in Fig. 5.2a. The green line indicates where a simulated and predicted value would match. The larger the distance from the bisecting line, the larger the error gets. Values below the green line are estimated with a too low vorticity value. This especially happens for the high vorticity DNS results. At these high values, the number of simulations in the training set is not high enough to present the network with sufficient training data. Hence, the network is under-performing in these vorticity regions. Domains challenged the network where almost no cross-flow vortex was formed by the roughness patch.

5.3. Sensitivity Analysis

We performed a sensitivity analysis in order to understand the influence of single and multiple geometric input factors on the capability of the DNN to predict the streamwise vorticity. We measured the difference in the achieved mean error between the complete database and a reduced database where single or multiple input parameters were omitted.
An overview of the sensitivity analysis can be be found in Tab. 3. First, we tested the influence of every single parameter being excluded. This exclusion lead to a maximum increase of 7.32% of the mean error of DNN prediction. Especially the location of the maximum, the streamwise position of the minimum and the rms value of the roughness height are contributing significantly to the network. We underlined the importance of the rms roughness value in [6].
Further, we selected groups of parameters that we derived from the same geometrical parameter, for example all input parameters that we computed with streamwise derivative. In Tab. 3, these groups of parameters are positioned in the second group. Here, we see the importance for the prediction of maxima and minima positions and also the derivatives. Since there is a connection between the streamwise and spanwise derivative, the DNN can comprehend the omission of one directional derivative. However, the error increases by 24.41% when all factors derived from the directional derivatives are missing in the database.
The last group in Tab. 3 refers to input parameters which are derived from all geometrical features but with different statistical features, such as the maximum or rms value. All parameters contribute to the prediction with rms parameter being the most influential.
Finally, we see that not all parameters are necessary. The omission of certain parameters reduces the error further. However, this is only happening in the single-factor group and is due to over-fitting. It would be beneficial to only include the average value of the spanwise derivative, but not also the maximum, the rms-value and the skewness.

With the investigated combinations, we can see the importance of the surface derivatives as well as the position of the surface maxima and minima. Also, the rms roughness height

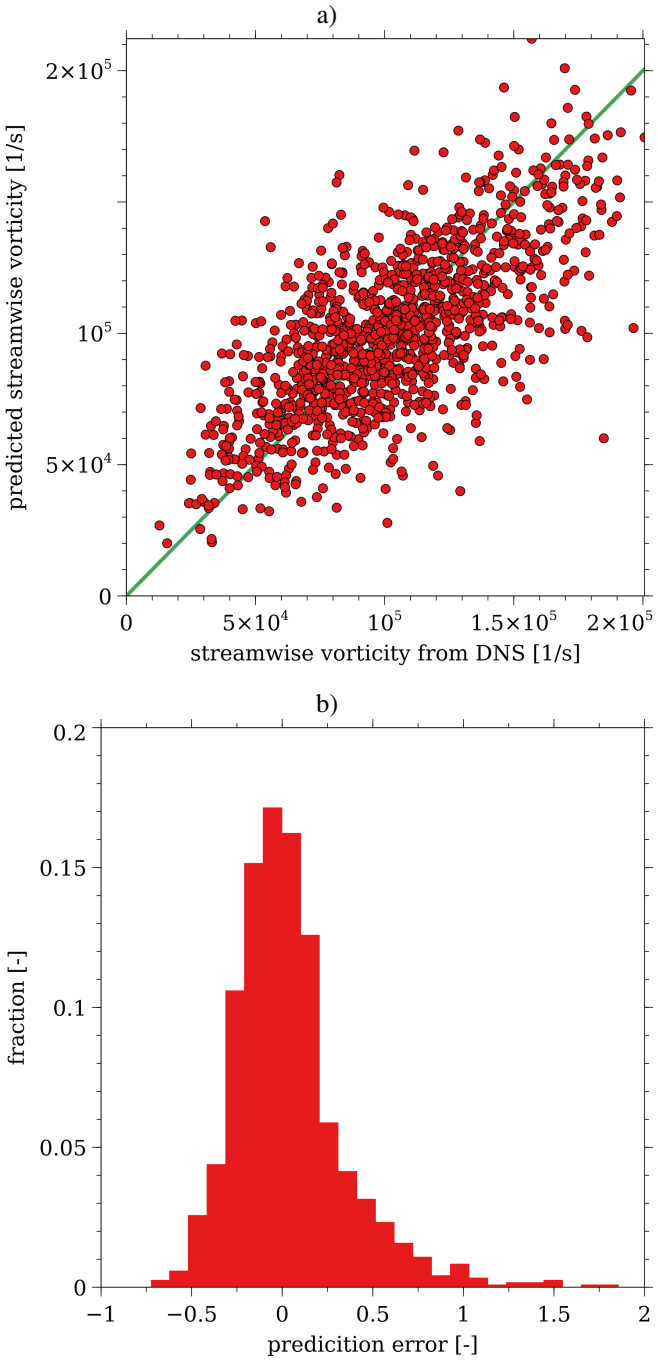

Fig. 4. comparison between predicted an simulated data (a) and DNN error histogram (b)

is contributing to the prediction. Further, it is necessary to reduce the number of parameters derived from the same geometrical feature to prevent over-fitting.

Table 3. Sensitivity analysis

removed parameter(s)	ΔError [%]
h_{avg}	-1.52
$curv(h)_{mean,avg}$	-1.09
$curv(h)_{gauss,avg}$	-1.81
$\partial h/\partial i_{avg}$	-0.16
$\partial h/\partial k_{avg}$	2.77
h_{max}	4.94
$curv(h)_{mean,max}$	-1.05
$curv(h)_{gauss,max}$	2.61
$\partial h/\partial i_{max}$	0.43
$\partial h/\partial k_{max}$	-0.82
h_{rms}	**5.84**
$curv(h)_{mean,rms}$	0.93
$curv(h)_{gauss,rms}$	3.01
$\partial h/\partial i_{rms}$	2.71
$\partial h/\partial k_{rms}$	-1.63
$Sk(h)$	2.94
$Sk(curv(h)_{mean})$	-1.59
$Sk(curv(h)_{gauss})$	1.72
$Sk(\partial h/\partial i)$	0.17
$Sk(\partial h/\partial k)$	-1.18
I_x	-0.88
I_z	-3.00
$Pos_{max,i}$	**7.32**
$Pos_{max,k}$	**6.61**
$Pos_{min,i}$	**5.22**
$Pos_{min,k}$	-0.75
all heights	**7.80**
all derivatives	**24.41**
all $\partial h/\partial i$	**8.71**
all $\partial h/\partial k$	4.30
I_i,I_k	1.76
all positions	**22.88**
all curvature	4.30
all average	0.59
all maximum	1.31
all rms	**6.28**
all skewness	0.64

5.4. Reduction of Roughness Peak Height

In this section, the peak height is reduced and the effect on the streamwise vorticity is analyzed. An increase in the roughness peak height does also change the derivatives on the roughness surface as well as the other roughness parameters. The decrease of the roughness peak height will not lead to a change in the position of the maximum and minimum peak height. The sensitivity analysis identifies the derivative parameter and the maximum and minimum position as the most influential parameter. Hence, this section also investigates the change in geometrical roughness parameters but with a

constant maximum/minimum location.
The original database had a roughness peak height to boundary-layer height ratio of $h_{max}/\delta = 0.18$. A second set of simulations is performed with $h_{max}/\delta = 0.148$, a reduction of 21% of the peak height.
In Fig. 5a, the vorticity distribution of both databases is plotted. The lower peak height database (black) is shifted towards lower vorticity values compared to the higher peak database in red. The most common vorticity value is reduced by half from $\approx 100k$ 1/s to $\approx 50k$ 1/s.

Further, we picked a random set of simulations from the

Table 4. Overview over two domains with different peak height

h_{max}/δ	ω_x [1/s]	vortex core y-Pos. [mm]	vortex core z-Pos. [mm]
0.18	148,537.23	5.7	-19.1
0.148	112,374.57	3.5	-17.3
Δh_{max}	$\Delta\omega_x$ [%]	ΔPos_y [%]	ΔPos_z [%]
21	32	62	10

database to compare the flow field of the same roughness patch differing only in the maximum roughness-peak height side by side. The position of the roughness peaks and valleys is the same for these patches. The streamwise velocity is displayed in Fig. 5b for both roughness peak heights for the same roughness patch. Both patches show a similar flow field where no cross-flow-like vortex is present. Also the spanwise location of the vortices does change by only 10% when the peak height is reduced. Nevertheless, an increase in vorticity of 32% is observed and the vortices are lifted from the wall further in the wall-normal direction. The y-position of the vortex core increases by 62%. An overview over two patches can be found in Tab. 4.

A database with decreased peak height leads to a general reduction of the maximum vorticity in the wake. We further observe that the wall-normal location of the vortex core is increasingly influenced by the change of the roughness parameter than the spanwise location with constant maxima/minima location. This corresponds to the results in Sec. 5.1 where the cross-flow vortex core is observed downstream the maximum roughness peak. If this peak is decreased, also spanwise derivatives decrease, but this has only little effect on the spanwise location of the vortex core in the wake.

6. SUMMARY

This investigation presents the generation of a large database of DNS (4830 simulations) for the prediction of streamwise vorticity of cross-flow like vortex in the wake of distributed random roughness patches. A suitable domain resolution was chosen to meet the required accuracy and reduce computational time.

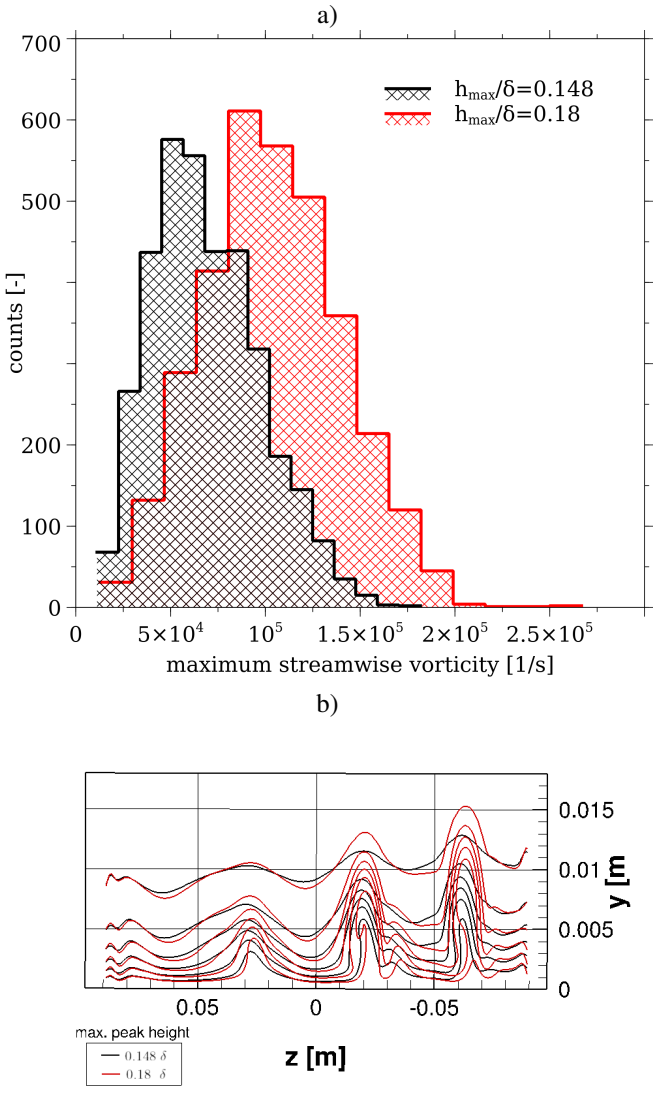

Fig. 5. a): histogram of streamwise vorticity distribution b): y-z-slice of streamwise velocities for $h_{max}/\delta = 0.18$ (red) and $h_{max}/\delta = 0.15$ (black)

From this database, a random set of two roughness grids are chosen and the baseflow of these simulation was displayed. The fluid is lifted by the maximum peak height in both simulations and forms a cross-flow like vortex downstream the maximum peak.
A DNN was trained with the database and tested with a separate set of simulations in a second step. The network is able to predict the maximum streamwise vorticity value in the wake with given roughness parameter with an average error.
A sensitivity analysis has revealed the surface derivatives as well as the position of the roughness maximum and minimum as the most influential parameter. Also using rms-values relative to skewness values of the geometric input parameter in-

creases the prediction capability of the DNN.
A second set of DNS was generated with a maximum peak height reduced by 18%. The maximum streamwise vorticity in the wake showed a similar distribution curve, but the curve is shifted towards lower vorticity magnitudes. As expected, the lower peak amplitude of the patch leads to a decrease in vorticity in the wake. By comparing two DNS with the roughness patch only differing in the maximum peak height, we see that the streamwise velocity is differing a lot in the vortex region while the rest of the flow field remains similar. Since the position of the maxima and minima remains the same compared to the other roughness parameter, we saw that the position of the vortex core is linked to the position of the maximum peak height.
In the future, the authors want to focus on the improvement of the precision of the DNN. A better performance can be achieved with cross-validation and increasing of the database size which will also further reduce over-fitting of the network. Certain products of input parameters could be used as new input might to further increase the performance. However, it is necessary not to overfit the network to the proposed database. Also the DNN itself could be optimized by hypertuning of network parameter such as the number and size of the hidden layers.

7. ACKNOWLEDGEMENTS

This research was supported by founds of the TUM International Graduate School of Science and Engineering (IGSSE) and the Cusanuswerk e.V scholarship. Further, the authors gratefully acknowledge the Gauss Centre for Supercomputing e.V. (www.gauss-centre.eu) for supporting this project by providing computing time on the GCS Supercomputer SuperMUC-NG at Leibniz Supercomputing Centre (www.lrz.de).

8. REFERENCES

[1] E. R. Van Driest, "The problem of aerodynamic heating," *Aeronautical Engineering Review*, vol. 15, no. 10, pp. 26–41, 1956.

[2] S. Hein, A. Theiss, A. Di Giovanni, C. Stemmer, T. Schilden, W. Schrder, P. Paredes, M. M. Choudhari, F. Li, and E. Reshotko, "Numerical investigation of roughness effects on transition on spherical capsules," *Journal of Spacecraft and Rockets*, vol. 56, no. 2, pp. 388–404, 2019.

[3] S. P. Schneider, "Effects of roughness on hypersonic boundary-layer transition," *Journal of Spacecraft and Rockets*, vol. 45, no. 2, pp. 193–209, 2008.

[4] I. Padilla Montero and F. Pinna, "Analysis of the instabilities induced by an isolated roughness element in a laminar high-speed boundary layer," *Journal of Fluid Mechanics*, vol. 915, pp. A90, 2021.

[5] A. Di Giovanni and C. Stemmer, "Cross-flow-type breakdown induced by distributed roughness in the boundary layer of a hypersonic capsule configuration," *Journal of Fluid Mechanics*, vol. 856, pp. 470–503, 2018.

[6] F. Ulrich and C. Stemmer, "Investigation of vortical structures in the wake of pseudo-random roughness surfaces in hypersonic reacting boundary-layer flows," *International Journal of Heat and Fluid Flow*, vol. 95, pp. 108945, 2022.

[7] S. L. Brunton, B. R. Noack, and P. Koumoutsakos, "Machine learning for fluid mechanics," *Annual Review of Fluid Mechanics*, vol. 52, no. 1, pp. 477–508, 2020.

[8] M. Aghaei Jouybari, J. Yuan, G. J. Brereton, and M. S. Murillo, "Data-driven prediction of the equivalent sand-grain height in rough-wall turbulent flows," *Journal of Fluid Mechanics*, vol. 912, pp. A8, 2021.

[9] S. Lee, J. Yang, P. Forooghi, A. Stroh, and S. Bagheri, "Predicting drag on rough surfaces by transfer learning of empirical correlations," *Journal of Fluid Mechanics*, vol. 933, pp. A18, 2022.

[10] C. Park, "A review of reaction rates in high temperature air," in *24th Thermophysics Conference*. AIAA paper 89 - 1740, June 1989.

[11] A. Di Giovanni and C. Stemmer, "Roughness-induced boundary-layer transition on a hypersonic capsule-like forebody including nonequilibrium," *Journal of Spacecraft and Rockets*, vol. 56, no. 6, pp. 1795–1808, 2019.

[12] A. Di Giovanni and C. Stemmer, "Roughness-induced crossflow-type instabilities in a hypersonic capsule boundary layer including nonequilibrium," *Journal of Spacecraft and Rockets*, vol. 56, no. 5, pp. 1409–1423, 2019.

[13] J. B. Vos, N. Duquesne, and H. J. Lee, "Shock wave boundary layer interaction studies using the NSMB flow solver," in *Third European Symposium Aerothermodynamics for Space Vehicles*, 1999, vol. 426, p. 229.